Tellus (1996), 48A, 483–500
Printed in UK – all rights reserved

TELLUS
ISSN 0280–6495

A mixed-phase cloud scheme based on a single prognostic equation

By ANDRÉ TREMBLAY[1,*], ANNA GLAZER[1], WEI YU[2], and ROBERT BENOIT[3] *Atmospheric Environment Service, [1]Cloud Physics Research Division, [2]Data Assimilation and Satellite Meteorology Division, [3]Division de Recherche en Prévision Numerique, 2121 Trans Canada Highway, Dorval, Qc, Canada, H9P 1J3*

(Manuscript received 28 September 1995; in final form 19 February 1996)

ABSTRACT

A mixed-phase cloud scheme is proposed. It is derived by considering simplifications from cloud microphysics parameterizations currently used in cloud models. The scheme considers only one prognostic variable (the total water content) partitioned diagnostically into solid and liquid phases at subfreezing temperatures. The scheme preserves the basic microphysical processes characterizing natural mixed-phase clouds and does not include any adjustable (nonphysical) parameter. The proposed approach can be used in mesoscale or large-scale atmospheric models since it is computationally fast and easy to implement. This allows simulations that would have been otherwise impossible with more elaborate cloud microphysics schemes, because of excessive computational load. Numerical experiments with a mesoscale model have shown that mixed-phase clouds generated with the scheme are confined to localized regions and are strongly correlated with the intensity of the vertical lifting. The amount of supercooled liquid water (SLW) thus obtained is substantially less than the amount obtained from other schemes using temperature as the only indicator for the appearance of mixed-phase clouds.

1. Introduction

Clouds and precipitation play a fundamental role in the evolution of weather processes. For example, North American winter storms are commonly characterized by a wide range of cloud and precipitation types including rain, snow, ice pellets, snow pellets, snow grains, freezing rain or drizzle and often a mixture of these (Stewart and Crawford, 1995). To produce reliable weather forecasts, it is essential to include these various weather elements in numerical weather prediction (NWP) models.

The importance of clouds and precipitation has also been widely recognized in climate processes. Since the radiative properties of clouds are strong functions of their water content, the phase of the water and particle size distribution, their parameterization is an important aspect to consider in atmospheric general circulation models (GCM). Thus NWP models and GCMs tend to evolve from very crude diagnostic representation of clouds to more elaborate physically based prognostic schemes (Tiedtke, 1993).

Following basic principles formulated by Kessler (1969) several parameterization schemes of cloud microphysics were introduced in cloud resolving models (CRM) (Koenig and Murrray, 1976; Orville and Kopps, 1977; Lin et al., 1983; Zawadzki et al., 1993). These schemes consider an individual prognostic equation for each form of water substance and explicitly represent microphysical processes that account for specific intercategorical transport. For example Rutledge and

* Corresponding author.

Hobbs (1984) considered conservation equations for cloud water, cloud ice, rain, snow and graupel with 22 different microphysical processes. The schemes including several cloud prognostic variables are very expensive and computer limitations usually prevent their incorporation in large-scale models. For this reason, NWP models and GCMs currently tend to implement more efficient cloud schemes (Sundqvist, 1978; Smith 1990; Roads et al. 1984).

Sundqvist (1978) introduced a new concept for the treatment of cloud and precipitation processes in atmospheric models. He considered only the cloud water content as a prognostic variable and elegantly formulated sub-grid condensation (the scheme allows fractional cloudiness within a grid box). The rate of conversion of cloud droplets into precipitation-sized particles was also introduced along with the assumption that precipitation falls instantly at the surface as it forms aloft. Sundqvist (1981) used the scheme in conjunction with the ECMWF global model and the results were validated against satellite pictures. Sundqvist et al., (1989) implemented the same scheme in the mesoscale model of the Norwegian Meteorological Institute and obtained improved forecasts compared to the original model formulation.

Smith (1990) implemented a single variable cloud scheme in the UK Meteorological Office atmospheric general circulation model. His scheme generally goes in a direction parallel to Sundqvist, but the subgrid condensation follows concepts developed by Sommeria and Deardorff (1977) and Mellor (1977). The scheme also includes a treatment of mixed-phase clouds, an important characteristic of cloud microphysics. At subfreezing temperatures, the partition of the condensate into SLW and ice crystals is assumed to be a function of temperature only. Smith (1990) suggests a quadratic spline to obtain a smooth transition from a totally glaciated cloud at $-15°C$ to a liquid cloud at 0°C. The temperature dependence of the fractional ice content has been adjusted without physical basis to tune the model since "*Excessive cloud was simulated if liquid water was assumed to exist below $-15\,°C$*". In a more recent work, Sundqvist (1993) generalized his scheme to account for mixed-phase clouds. He also assumes that the fractional amount of ice crystals in a mixed-phase volume is a function of temperature only. Sundqvist (1993) completed his formulation with the statistical data of Matveev (1984) to establish the temperature dependence of the fractional ice content.

Since important differences exist between physical properties of ice and warm clouds, a physically meaningful treatment of mixed-phase clouds in atmospheric models is needed. It is felt that existing schemes oversimplify the physics of mixed-phase clouds and do not account for the highly transient nature of the Bergeron-Findeisen process. In this paper an alternative mixed-phase cloud scheme is suggested for use in mesoscale or large-scale atmospheric models. The scheme is based on a single prognostic equation, and is derived from a consistent simplification of more elaborate parameterization schemes currently considered in CRMs. Only one prognostic cloud variable, the total condensate, is included and the fractional ice content is obtained diagnostically as a function of several parameters accessible from any atmospheric model. The proposed diagnostic relationship could also be used as an alternative framework with the above mentioned schemes for incorporating mixed-phase clouds.

For the moment, the scheme is totally explicit which means that neither subgrid scale condensation nor subgrid scale convection is considered. However, the importance of these processes has been widely recognized and they are taken into account in large-scale cloud schemes (e.g., see citations above and references therein). This limits the application of the present scheme to resolutions which explicitly resolve these processes (mesoscale at best). Thus, parameterization of these subgrid processes must be considered for larger-scale applications of the present scheme. For this reason, numerical integrations discussed in this paper will be limited to high resolution simulations, larger-scale applications being left for the future.

This article is organized as follows. The mixed-phase cloud scheme is elaborated in Section 2. The general context for the application of the scheme is outlined in Section 3. To illustrate the basic characteristics of the cloud scheme for typical atmospheric situations, simple one-dimensional layer cloud simulations are briefly discussed in Section 4. Finally, to provide an example of the behavior of the present cloud scheme on the mesoscale, a numerical experiment using the Canadian MC2 (Mesoscale Compressible

Community) model is briefly discussed in Section 5.

2. Cloud scheme

2.1. Mixed phase in saturated updrafts

Assuming a saturated updraft layer at a subfreezing temperature, consider the following model for the time evolution of condensed water phases:

$$\frac{dq_L}{dt} = C - R + \Phi_L - q_L \nabla \cdot V, \tag{1}$$

$$\frac{dq_S}{dt} = D + R + \Phi_S - q_S \nabla \cdot V, \tag{2}$$

where q_L and q_S are respectively the liquid and solid water content (q_L and $q_S > 0$ is assumed), C the condensation rate, D the vapor deposition on ice crystals, R the interaction between the liquid and solid phases (riming) and Φ_L, Φ_S symbolize the sedimentation terms. The terms involving the divergence of the air velocity ($\nabla \cdot V$) are explicitly included since the problem is formulated in terms of density units rather than mixing ratios. In cloud microphysics models (Cotton and Anthes, 1989; Houze, 1992; Lin et al., 1983; Rutledge and Hobbs, 1984), the various forms of water substance in a cloud are generally subdivided into a larger number of categories. Thus, the categories embodied in q_L encompass the total liquid phase including cloud water, drizzle and rainwater, and q_S includes all solid particle species. Eqs. (1) and (2) are formally derived by adding individual equations for each water substance category, since inter-category transport terms identically vanish.

Mixed-phase clouds are saturated with respect to water implying an equilibrium in which supersaturation production is balanced by condensation on droplets and deposition on ice crystals. From detailed cloud microphysics simulations, Tremblay et al., (1995) have demonstrated that within mixed-phase clouds the following relationship is valid with a high degree of accuracy:

$$wG = C + D, \tag{3}$$

where w is the vertical velocity, and $-G$ is the product of air density with the vertical gradient of the saturation mixing ratio with respect to water (Kessler, 1969). The relation (3) implies that the production of supersaturation due to adiabatic cooling is the dominant source for supersaturation which is almost exactly in equilibrium with condensation and deposition. Physically, wG represents the generation of water vapor excess over saturation by moist adiabatic cooling. G is a function of temperature and pressure and using the Clausius-Clapeyron equation it can be shown that:

$$G(T,p) = \rho r_s \left(\frac{L_v}{R_v T^2} \Gamma_w - \frac{g}{R_d T} \right), \tag{4}$$

where r_s is the saturation mixing ratio, Γ_w the wet adiabatic lapse rate, L_v the latent heat of vaporization, T the ambient temperature, g the gravitational acceleration, R_d and R_v the gas constants for dry air and water vapor respectively and ρ is the air density.

Adding (1) and (2) and using (3) gives an equation for the time evolution of the total condensate $M = q_L + q_S$:

$$\frac{dM}{dt} = wG + \Phi_S + \Phi_L - M \nabla \cdot V. \tag{5}$$

To close (5) for M, explicit forms for the sedimentation terms Φ_L and Φ_S must be introduced. Following Colton (1976) the sedimentation of the single prognostic variable M can be expressed as:

$$\Phi_{MM} = -\frac{\partial (M V_M)}{\partial z}, \tag{6}$$

which is the vertical divergence of the M-flux.

The effective fallspeeds of the liquid and solid phases are:

$$V_M = \begin{cases} aM^b \left(\dfrac{\rho_0}{\rho}\right)^{1/2} \equiv V_S, & \text{for solid phase}, \\ cM^d \left(\dfrac{\rho_0}{\rho}\right)^{1/2} \equiv V_L, & \text{for liquid phase}, \end{cases} \tag{7}$$

where $\rho_0 = 1$, ρ is the air density and a, b, c and d are empirical constants (Ogura and Takahashi, 1971). Colton (1976) used this scheme in a mesoscale model to simulate precipitation distribution in the Sierra Nevada mountains. His results clearly demonstrate that this simplified method gives good results when compared to surface observations. Even if (6) introduces a significant simplification when compared to the formalism of CRMs it still nevertheless constitutes a refinement with

Table 1. *List of symbols*

Symbol	Description	Value and units
ρ	air density	$kg\ m^{-3}$
ξ	mixed-phase sedimentation parameter	dimensionless
π	3.14159...	
Δ	coefficient of diffusion of water vapor in air (Rogers, 1979)	$2.11 \times 10^{-5}\ m^2\ s^{-1}$
τ	time scale	arbitrary time unit
Φ	total sedimentation term (eq. 23)	$g\ m^{-3}\ s^{-1}$
β	Fletcher's constant (Fletcher, 1962)	$0.6\ K^{-1}$
ρ_0	reference air density	$1\ kg\ m^{-3}$
μ_0	mass of an ice crystal after nuclei activation (Zawadzki et al. 1993)	$10^{-9}\ g$
ν_0	Fletcher's constant (Fletcher, 1962)	$10^{-2}\ m^{-3}$
β_1	empirical constant relating the first moment of solid particle size distribution to its third moment (Zawadzki et al. 1993)	0.58
α_1	empirical constant relating the first moment of solid particle size distribution to its third moment (Zawadzki et al. 1993)	55.63 $mm^{(1-3\beta_1)}\ m^{3(\beta_1-1)}$
β_2	empirical constant relating the $(2+b)^{th}$ moment of solid particle size distribution to its third moment (Zawadzki et al. 1993)	0.79
α_2	empirical constant relating the $(2+b)^{th}$ moment of solid particle size distribution to its third moment (Zawadzki et al. 1993)	3.45 $mm^{2+b-3\beta_2}\ m^{3(\beta_2-1)}$
Γ_d	dry adiabatic lapse rate	$9.8°C\ km^{-1}$
Φ_L	liquid sedimentation term (eq. 1)	$g\ m^{-3}\ s^{-1}$
Φ_{ML}	liquid sedimentation term	$g\ m^{-3}\ s^{-1}$
Φ_{MS}	solid sedimentation term	$g\ m^{-3}\ s^{-1}$
ν_n	number of ice nuclei per unit volume	m^{-3}
Φ_S	solid sedimentation term (eq. 2)	$g\ m^{-3}\ s^{-1}$
Δt	time step	s
Γ_w	moist adiabatic lapse rate	$°C\ km^{-1}$
a	constant in empirical formula for V_S (Ogura and Takahashi, 1971)	-5.9×10^{-6b} $g^{-b}\ m^{1+3b}\ s^{-1}$
a_1	constant in formula for c_R (Zawadzki et al. 1993)	$147\ cm^{0.73}\ s^{-1}$
b	constant in empirical formula for V_S (Ogura and Takahashi, 1971)	0.11
C	condensation rate	$g\ m^{-3}\ s^{-1}$
c	constant in empirical formula for V_L (Ogura and Takahashi, 1971)	-31.2×10^{-6d} $g^{-d}\ m^{1+3d}\ s^{-1}$
C_3	constant for units transformation	$2 \times 10^4\ mm^3\ g^{-1}$
c_p	specific heat of air at constant pressure	$1005\ J\ kg^{-1}\ K^{-1}$
D	vapor deposition rate on ice crystals	$g\ m^{-3}\ s^{-1}$
d	constant in empirical formula for V_L (Ogura and Takahashi, 1971)	0.125
E	evaporation rate of liquid phase	$g\ m^{-3}\ s^{-1}$
E_{SC}	collection efficiency of water droplets by solid particles	1
e_{si}	saturation vapor pressure over ice	Pa
f	fractional ice content	dimensionless
f_s	fractional ice content at steady state	dimensionless
f_v	ventilation coefficient	1
G	negative of the product of air density with the vertical gradient of the saturation mixing ratio	$kg\ m^{-4}$
g	acceleration of gravity	$9.8\ m\ s^{-1}$
K	thermal conductivity of air	0.0236 $J^{-1}\ m^{-1}\ s^{-1}\ K^{-1}$
k_E	constant for evaporation (Kessler, 1969)	5.53×10^{-4}

Table 1. *List of symbols (Continued)*

Symbol	Description	Value and units
k_L	liquid phase autoconversion threshold	$0\ \mathrm{g\ m^{-3}}$
k_S	solid phase autoconversion threshold	$0\ \mathrm{g\ m^{-3}}$
L_s	latent heat of sublimation	$2.834\times10^6\ \mathrm{J\ kg^{-1}}$
L_v	latent heat of vaporization	$2.501\times10^6\ \mathrm{J\ kg^{-1}}$
M	mass density of condensate	$\mathrm{g\ m^{-3}}$
N	nucleation rate	$\mathrm{g\ m^{-3}\ s^{-1}}$
p	pressure	Pa
q_L	liquid water content	$\mathrm{g\ m^{-3}}$
q_S	solid water content	$\mathrm{g\ m^{-3}}$
q_v	vapor content	$\mathrm{g\ m^{-3}}$
q_{vs}	saturation vapor content	$\mathrm{g\ m^{-3}}$
R	riming rate	$\mathrm{g\ m^{-3}\ s^{-1}}$
r	relative deviation of f from f_s	dimensionless
R_d	gas constant for dry air	$287.05\ \mathrm{J\ kg^{-1}\ K^{-1}}$
r_s	saturation mixing ratio	dimensionless
r_{si}	saturation mixing ratio with respect to ice	dimensionless
R_v	gas constant for moist air	$461.51\ \mathrm{J\ kg^{-1}\ K^{-1}}$
S_i	saturation ratio relative to ice	dimensionless
T	temperature	°C or K
T_0	freezing temperature	273.15 K
V	air velocity vector	$\mathrm{m\ s^{-1}}$
V_L	terminal fallspeed of the liquid phase	$\mathrm{m\ s^{-1}}$
V_S	terminal fallspeed of the solid phase	$\mathrm{m\ s^{-1}}$
w	vertical velocity	$\mathrm{m\ s^{-1}}$
w_1	vertical velocity threshold	$\mathrm{m\ s^{-1}}$
z	vertical coordinate	m

respect to many NWP models. For example, in the Sundqvist scheme it is assumed that the precipitation falls instantly at the surface as it forms aloft. Colton's formulation does not account for mixed-phase clouds: the solid phase is inferred for temperatures below freezing ($M=q_S$), and liquid water for $T>0$°C ($M=q_L$). In the present investigation, we consider mixed-phase clouds and assume that Φ_L and Φ_S are given by:

$$\Phi_L=(1-f)\Phi_{ML}\,, \tag{8}$$

$$\Phi_S=f\Phi_{MS}\,, \tag{9}$$

where Φ_{ML} and Φ_{MS} are given by (6) with $V_{M=}V_L$ and V_S, respectively, and the parameter f is defined as the fractional ice content of M,

$$q_L=(1-f)M\,, \tag{10}$$

$$q_S=fM\,. \tag{11}$$

With this treatment of sedimentation, the condensate always precipitates for any value of $M>0$. Thus, the initial phase of cloud formation, when suspended particles with low water content exist before the onset of precipitation, is not included in the present formulation. It is however possible to crudely account for this effect by considering:

$$\Phi_{ML}=\begin{cases}-\dfrac{\partial}{\partial z}\left[c(M-k_L)^{1+d}\left(\dfrac{\rho_0}{\rho}\right)^{1/2}\right] & \text{for } M>k_L,\\ 0 & \text{for } M\leqslant k_L,\end{cases} \tag{12}$$

$$\Phi_{MS}=\begin{cases}-\dfrac{\partial}{\partial z}\left[a(M-k_S)^{1+b}\left(\dfrac{\rho_0}{\rho}\right)^{1/2}\right] & \text{for } M>k_S,\\ 0 & \text{for } M\leqslant k_S,\end{cases} \tag{13}$$

where (6) and (7) were used to derive (12) and (13). Constants k_L and k_S are similar to the *autoconversion threshold* of Kessler (1969). However since we have only one prognostic equation the time constant of the autoconversion process should tend to infinity. For constant particle fallspeeds, in an incompressible atmosphere

(b, $d=0$; $\rho=\rho_0$), (12) and (13) are independent of the specific values of k_L and k_S. For the numerical simulations discussed in the following sections the focus is on precipitation systems associated with synoptic storms, so $k_L=k_S=0$.

2.2. Evolution of the fractional ice content

It is possible to obtain an equation for the evolution of the fractional ice content by differencing (11), and using (2), (5), (8) and (9):

$$\frac{df}{dt}=\frac{D+R}{M}-\frac{wG}{M}f[1+(1-f)\xi], \tag{14}$$

where the non-dimensional parameter ξ represents the net effect of mixed-phase sedimentation and is given by:

$$\xi=\frac{\Phi_{ML}-\Phi_{MS}}{wG}. \tag{15}$$

To derive an explicit form of (14) we need to express D and R in terms of M and f. Assuming a mixed cloud saturated with respect to water, and assuming that solid particles are distributed in size according to empirical relationships given by Zawadzki et al. (1993), it can be shown that the vapor deposition on ice crystals D is:

$$D(f,M,T)=c_D(T)M^{\beta_1}f^{\beta_1}, \tag{16}$$

where:

$$c_D(T)=\frac{2\pi(S_i(T)-1)}{\dfrac{L_s^2}{KR_vT^2}+\dfrac{R_vT}{e_{si}(T)\Delta}}(f_v\alpha_1C_3^{\beta_1}), \tag{17}$$

and $S_i=e_s/e_{si}$ is the ratio of the saturation vapor pressure over water and ice, L_s the latent heat of sublimation, K the coefficient of thermal conductivity of air, Δ the coefficient of diffusion of water vapor in air, $f_v=1$ the ventilation coefficient, α_1 and β_1 are empirical constants, and C_3 is a coefficient for units transformation (see Table 1 for the list of symbols).

Following classical procedures (outlined in Cotton and Anthes, 1989; Houze, 1992 and Zawadzki et al., 1993), an expression for the riming function R is obtained:

$$R(f,M,T,p)=c_R(T,p)M^{1+\beta_2}f^{\beta_2}(1-f), \tag{18}$$

where:

$$c_R(T,p)=\frac{\pi}{4}E_{SC}\left(\frac{\rho_0}{\rho}\right)^{1/2}a_1C_3^{\beta_2}\alpha_2. \tag{19}$$

Here $E_{SC}=1$ is the collection efficiency of water droplets by solid particles and a_1, β_2 and α_2 are empirical constants (Table 1).

Eqs. (16) and (18) parameterize D and R in terms of empirically-derived mass-moments relationships for the solid particle-size distribution (Zawadzki et al., 1993). D, which depends on the first moment of the particle-size distribution, is related to M by a least-square regression in log-log coordinates via a relationship of the form $\alpha_1M^{\beta_1}$. Similarly, R depends on the $(2+b)$ moment which is related to M through a relationship of the form $\alpha_2M^{\beta_2}$. There are of course uncertainties associated with α and β which are based only on few hours of data and the variability of these parameters is for the moment unknown. This emphasizes the need for a formal model validation and additional measurements, before attempting a generalization of the present scheme.

A substitution in (14) yields:

$$\frac{df}{dt}=c_DM^{\beta_1-1}f^{\beta_1}+c_RM^{\beta_2}f^{\beta_2}(1-f)$$
$$-\frac{wG}{M}f[1+(1-f)\xi]. \tag{20}$$

Eqs. (20) and (5) are strictly equivalent to (1) and (2) in regions where (3) is valid. The differential eq. (20) gives the rate of change of f with time within a volume containing a mass density M of condensate, with a temperature T, vertical velocity w, pressure p, and mixed-phase sedimentation ξ. Equilibrium solutions of (20) provide a diagnostic relationship for f in terms of these parameters.

The study of the transient solutions of (20) has important implications in the establishment of a diagnostic relationship for f. A knowledge of the time constants involved in the microphysics processes controlling the equilibrium value of f is crucial to assess the applicability of the diagnostic. Formally the integration of (20) would require simultaneous integrations of the equations that describe the tendency of M, T, w and p. However, a simplification is possible by assuming that f is determined by fast microphysical processes and M, T, w and p by slower processes mostly controlled by large-scale forcing. Thus, the characteristic time constants for f can be estimated by integrating (20) with constant values of all independent variables embodied in the right hand side of the equation. These time constants can be compared with typical time scales involved in large-scale processes to determine the range of applicability of the equilibrium solution of (20). Within this framework, time integrations are performed in a coordinate system moving with the flow, and Lagrangian time scales are obtained.

The independent variables embodied in the right hand side of (20) have their physical meaning, and remain within a limited range of values. The dependence on pressure p is the weakest. The choice of 800 mb level for figures 1 up to 5, presenting the solutions of (20), does not influence the conclusions. The temperature T remains within $[-20°\mathrm{C}, 0°\mathrm{C}]$ interval, as for temperatures below $-20°\mathrm{C}$ solid phase is assumed ($f=1$) and for T above 0°C liquid phase is expected ($f=0$). The range of w considered is $[0\ \mathrm{m\ s^{-1}}, 0.5\ \mathrm{m\ s^{-1}}]$ and it safely delineates typical values for mesoscale applications. The condensate M is assumed to be initially present, $M>0$, and a value of $1\ \mathrm{g\ m^{-3}}$ is chosen as its upper threshold value. It is difficult to estimate the range of variability of ξ, since it depends on the vertical structure of M, the intensity of the updraft, the air temperature and pressure. For the example given above (incompressible atmosphere and constant particle fallspeeds $V_S \neq V_L$), $\xi=0$ implies that M is uniform in z. In this work, the ξ-range was established from detailed diagnostic analyses of the numerical integrations discussed in Sections 4, 5 below. It has been found that the mixed phase sedimentation ξ mostly remains within the $[-1,1]$ interval. This interval will be used to illustrate the sensitivity of the equilibrium solution of (20) to this parameter (Fig. 5). Examples of the transient solution of (20) will be given for $\xi=0$ (Figs. 1–3). It is noteworthy that atmospheric calculations discussed in this paper consider the general case $\xi \neq 0$ and are not only limited to $\xi=0$.

Fig. 1a depicts the time evolution of the fractional ice content f for a total water content $M=0.3\ \mathrm{g\ m^{-3}}$, a temperature $T=-5°\mathrm{C}$, a pressure $p=800$ mb, and with $\xi=0$. The transient solutions are indexed for selected values of the vertical velocity typical of mesoscale. The figure indicates that the fraction of ice decreases as the updraft intensity increases. This can be explained by noting that in (20) the source term of SLW depends explicitly on w. The two other terms in the equation tend to deplete SLW by riming and deposition and are independent of w. Physically, increasing w at fixed M, increases the production of supersaturation without affecting its depletion. Since no supersaturation is allowed, this excess must go in the supercooled category. For this specific example, the initial value problems (IVP) were initialized with $f(0)=1$, and for each value of vertical velocity the solution converges quickly to an equilibrium value f_s. Clearly, the time interval for $f(t)$ to converge to f_s depends on the distance between $f(0)$ and f_s, or in other words, the time constant of the process is a function of the initial condition, a characteristic of many IVP. The curves in Fig. 1a show that the adjustment time to equilibrium is close to zero for $w=0.10\ \mathrm{m\ s^{-1}}$, and about 10 min for $w=0.40\ \mathrm{m\ s^{-1}}$, a large value for mesoscale circulations. This does not mean that the equilibrium approximation is better for small values of w, but only reflects the fact that the integration was started with an initial value close to f_s. Fig. 1b illustrates this, showing the same integrations with an initial condition $f(0)=0.5$. With such an initial condition the solution for $w=0.40\ \mathrm{m\ s^{-1}}$ tends to f_s more quickly than for

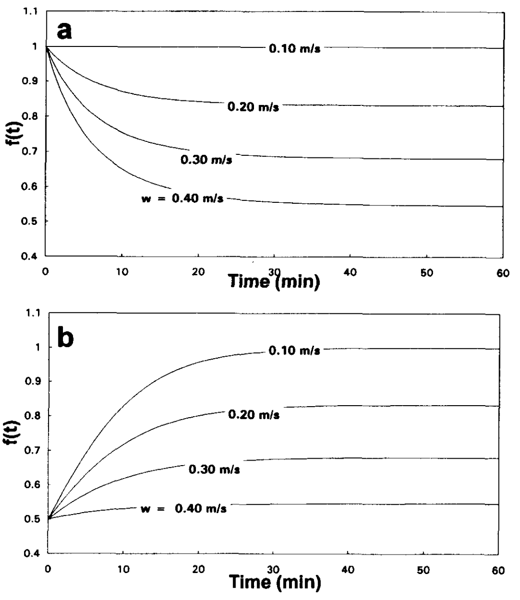

Fig. 1. (a) Fractional ice content as a function of time for a total water content $M=0.3\ \mathrm{g\ m^{-3}}$, at a temperature $-5°\mathrm{C}$, a pressure 800 mb and with $\xi=0$. The transient solutions initialized with $f(0)=1$ are displayed for several values of the vertical velocity. (b) As in (a) but initialized with $f(0)=0.5$.

$w = 0.10$ m s^{-1}. In general, when IVPs are initialized with values of $f(0)$ near 1, f_s is reached quickly for situations where ice phase predominates. Conversely, for cases where SLW is abundant, f_s is reached more rapidly when $f(0)$ is small. Physically, IVPs starting with $f(0) = 1$ represent cases where ice crystals at subfreezing temperatures exist in an updraft region. In such a region there is an equilibrium partition of M between SLW and ice phase, corresponding to the intensity of the updraft w. The other extreme, $f(0) = 0$, is for M initially consisting of only SLW, a case rarely observed in natural clouds (Cober et al., 1995).

To evaluate the deviation of the transient solution from equilibrium, consider:

$$r(\tau) = \frac{|f(\tau) - f_s|}{f_s}, \tag{21}$$

where r represents the normalized distance from f to f_s after a time τ. When r is small and τ is short compared to other characteristic time scales of NWP models or GCMs, the equilibrium solution of (20) provides an acceptable diagnostic for f. For example, for synoptic-scale flows considered in this paper, the disturbances last several days and representative time scales are hours. On the other hand, small scale disturbances such as convection evolve on faster time scales of the order of a few minutes.

Fig. 2a depicts r for $\tau = 10$ minutes (a short time scale for synoptic disturbances) as a function of temperature T and total condensate M, for $w = 0.10$ m s^{-1}, $p = 800$ mb, and $\xi = 0$. This figure was obtained by solving a set of IVP for different values of $0 < M \leqslant 1$ g m^{-3} and $-20°\mathrm{C} \leqslant T \leqslant 0°\mathrm{C}$, covering a range of interest. For most of the domain in the M–T plane $r < 0.10$, suggesting that f_s is a good approximation for f, for time scales $\tau \geqslant 10$ minutes. For such situations it is possible to model mixed clouds by solving only the differential equation for the total condensate M, and use the diagnostic relation for f to infer the phase partitioning of M. This approach has the advantage of being computationally fast and easy to implement, two desirable attributes for mesoscale and large-scale atmospheric models. Fig. 2a also shows that $r_{\max} \approx 0.25$ for warm temperatures and small M. By solving these IVP with a different initial condition, it can be shown that the localization of $r_{\max}$ is dependent of $f(0)$, but its intensity

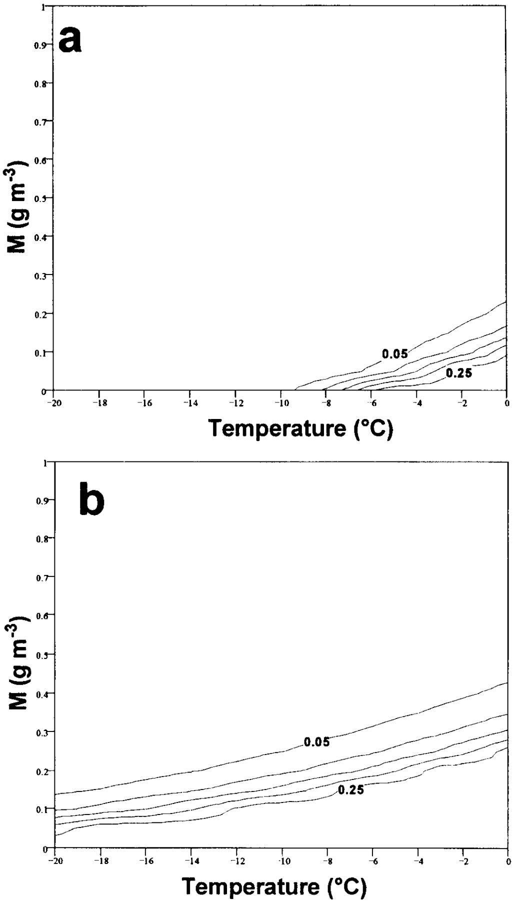

Fig. 2. (a) Deviation from equilibrium solutions after 10 min, as a function of temperature T and total water content M for $p = 800$ mb, $\xi = 0$ and $w = 0.10$ m s^{-1}. All initial value problems initialized with $f(0) = 1.0$. (b) As in (a) but for $w = 0.40$ m s^{-1}.

is mostly unaffected by this parameter. For example, the set of solutions obtained with $f(0) = 0.5$ results in a displacement of $r_{\max} \approx 0.25$ towards cold T, but the M–T plane remains mostly covered with $r < 0.10$. Fig. 2b shows that the equilibrium approximation becomes gradually poorer as vertical velocity increases to 0.40 m s^{-1}. For this case, as T approaches 0°C, r is in excess of 0.25 for $M < 0.3$ g m^{-3}, but $f = f_s$ remains a good approximation over a significant range of M and T. It is also worth mentioning that large w are more likely associated with large M, suggesting that f should remain close to f_s most of the time.

Other tests with different values of p and ξ indicate that the above conclusions are valid over a wide range of these parameters.

Since Fig. 2 indicates that the largest deviations of f from f_s are found for the smallest values of M, f_s is expected to be a good approximation for f within regions where the strongest meteorological signal is detected. Since numerical forecast models are generally more accurate in reproducing high liquid water content clouds rather than low liquid water content clouds, f_s can be considered as an acceptable approximation for f.

The equilibrium solution of (20) defines a partition of M into solid and supercooled liquid water phases, depending on specific values of M, T, w, ξ and p. Eq. (20) was solved at equilibrium for the vertical velocity w, and the results are reported in Fig. 3. The region in the f–w plane between isotherms 0°C and −20°C defines the domain of validity for the proposed model of fractional ice content f. The figure shows that for a given temperature, f decreases (SLW increases) as w increases. This illustrates that for large vertical velocities, the generation of supersaturation by adiabatic cooling is larger than the depletion of water vapor by deposition on solid particles. Fixing w in Fig. 3, indicates that the amount of SLW increases with T. There is an upper limit to the amount of SLW possible as T tends to 0°C, depending on the intensity of the vertical air current. Fig. 3 also illustrates how to diagnose the existence of SLW for given atmospheric conditions. At a given temperature, for all values of w below the intersection of a constant temperature curve and the line $f=1$, the depletion of water vapor by deposition is larger than the production by adiabatic cooling. In such a case, it is not possible to have SLW, and the cloud must be glaciated. The equilibrium solution of (20) for w, given M, T, p and $f=1$, is denoted by w_1:

$$w_1(M, T, p) = \frac{c_D(T) M^{\beta_1}}{G(T, p)}. \tag{22}$$

For all values of $w < w_1$, $f=1$, and the cloud is glaciated. Fig. 4 displays w_1 as a function of T and M for a constant pressure $p=800$ mb. For example, at a given temperature, the intensity of the updraft required to support SLW increases with M due to the larger potential amount of ice particles available to efficiently deplete water vapor.

Fig. 5 was generated by solving (20) numerically for f at equilibrium, and depicts the fractional ice content expressed as a function of temperature and total condensate for selected values of w and ξ. For a given point (M, T) in the diagrams of Fig. 5, the fractional ice content corresponds to specific values of w and ξ. For example, for $w = 0.50$ m s^{-1} and $\xi=0$, a mass of condensate $M = 0.4$ g m^{-3} at a temperature of −5°C would consist of 0.24 g m^{-3} (60%) of ice phase and 0.16 g m^{-3} of SLW. In each diagram, the isoline $f=1$, which

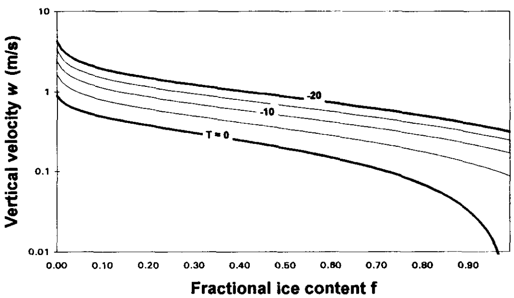

Fig. 3. Vertical velocity w (m s^{-1}) as a function of fractional ice content f for selected temperatures T(°C). $M = 0.3$ g m^{-3}, $p=800$ mb and $\xi=0$.

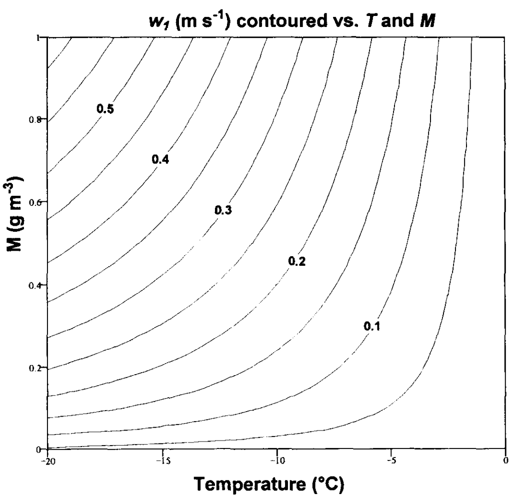

Fig. 4. Vertical velocity threshold w_1 (m s^{-1}) as a function of temperature T (°C) (abscissa) and total water content (g m^{-3}) (ordinate). A pressure of 800 mb was used for this calculation. At a given (M, T) point on the diagram SLW is possible only for situations where $w > w_1$.

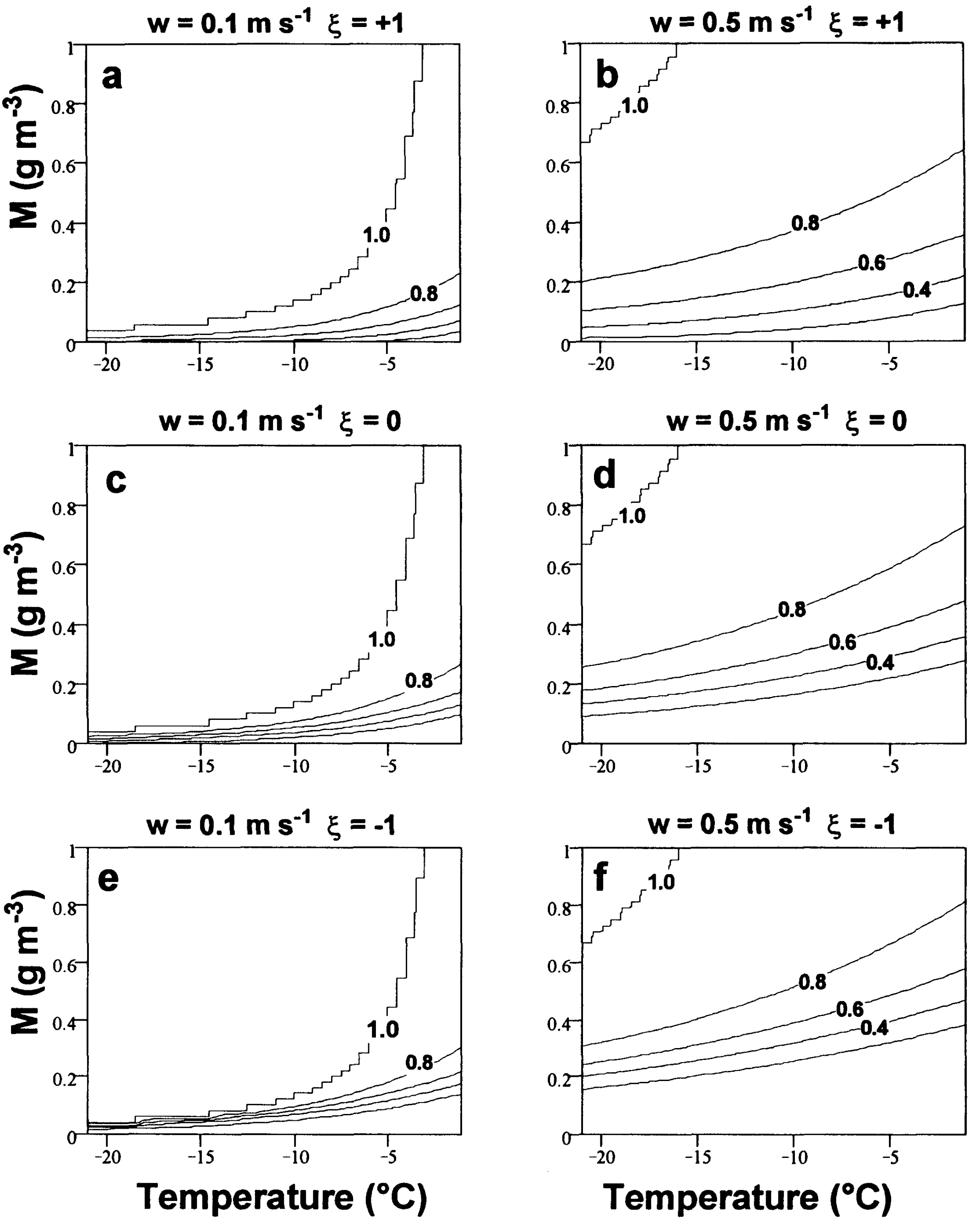

Fig. 5. Fractional ice content contoured as a function of temperature T (°C) (abscissa), total water content M (g m^{-3}) (ordinate), and for $p = 800$ mb.

defines the boundary between glaciated and mixed-phase clouds is independent of ξ and coincides with the corresponding w_1 isoline in Fig. 4. For fixed values of M and T, the figure demonstrates that f is a strong function of w. Comparably, the dependence on ξ is weaker, although significant. In any of the diagrams of Fig. 5, keeping M constant results in decreasing SLW amount with decreasing temperature as indicated by observations of clouds (Pruppacher and Klett, 1978 or Matveev, 1984). It is also apparent that the dependence of f on M is stronger than its dependence on T, as indicated by the shape of the f-isolines. From the above discussion $f = f(M, T, w, \xi, p)$, and trying to parameterize f in terms of T only may be questionable (Tremblay et al., 1994). This may be of potential interest for large-scale cloud parameterization using empirical functions of temperature to model f (Smith, 1990; Sundqvist, 1993), or for the interpretation of aircraft measurements for cloud parameterization development (Moss and Johnson, 1994).

3. Implementation of the cloud scheme in an atmospheric model

As already mentioned, only one prognostic cloud variable M, the total condensate expressed in mass density units, is considered. The condensate is liquid for $T \geqslant 0°C$ and solid or mixed for $T < 0°C$. If the conditions necessary for the existence of mixed phase are satisfied (i.e., saturated updraft $w > w_1$ and $T > -20°C$), the partitioning of M is done with the parameter f, the fractional ice content, given by the equilibrium solution of (20). Within such a framework, the governing equations for M, q_v and T are:

$$\frac{\mathrm{d}}{\mathrm{d}t}\begin{bmatrix} M \\ q_v \\ T \end{bmatrix} = \begin{bmatrix} (C+D+N+E)+\Phi \\ -(C+D+N+E) \\ \dfrac{L_v}{c_p}(C+E)+\dfrac{L_s}{c_p}(N+D) \end{bmatrix} - \begin{bmatrix} M\nabla\cdot V \\ q_v\nabla\cdot V \\ w\Gamma_d \end{bmatrix}. \tag{23}$$

Where Γ_d is the dry adiabatic lapse rate, Φ is the vertical divergence of the M flux given by (6) for either liquid Φ_{ML} or solid Φ_{MS} phases. For mixed-phase, Φ becomes the sum of Φ_L (8) and Φ_S (9). C is expressed in the form proposed by Asai (1965):

$$C = \frac{(q_v - q_{vs})/\Delta t}{1 + \dfrac{L_v^2 r_s}{c_p R_v T^2}}, \tag{24}$$

D is given by (16) and (17) with S_i defined here as the ratio of the actual vapor pressure to its saturation value over ice. D is zero for liquid phase, positive if the air is supersaturated with respect to ice and negative if subsaturation with respect to ice occurs and then represents sublimation.

In subsaturated regions large precipitation-sized particles evaporate at a finite rate (Kessler, 1969):

$$E = k_E(q_v - q_{vs})M^{0.65}, \tag{25}$$

where k_E is a constant.

Following Rutledge and Hobbs (1984) and Zawadzki et al. (1993), the initiation of M at subfreezing temperature is calculated from:

$$N = \min\begin{cases} \mu_0 \nu_n/\Delta t, \\ \dfrac{(q_v - q_{vsi})/\Delta t}{1 + \dfrac{L_s^2 r_{si}}{c_p R_v T^2}}, \end{cases} \tag{26}$$

where q_v is the water vapor content, q_{vsi} and r_{si} are the saturation vapor content and mixing ratio with respect to ice, μ_0 is the initial mass of an ice crystal after activation of freezing nuclei. Following Fletcher (1962) the number of activated freezing and sublimation nuclei per unit volume ν_n is:

$$\nu_n = \nu_0 \exp[\beta(T_0 - T)] \tag{27}$$

where ν_0 and β are empirical constants and $T_0 = 273.15$ K.

4. Layer cloud simulations

To illustrate the basic characteristics of the cloud scheme for typical atmospheric situations, simple numerical simulations are briefly discussed. It is assumed that an atmospheric layer of depth $H = 3$ km is initially saturated with respect to water. The base of this layer is at $p = 900$ mb with

$T = 4°C$. Within the layer, the temperature decreases linearly with z at a rate $= -3°C\ km^{-1}$ and the pressure is hydrostatic. This particular temperature profile was chosen to initiate both warm and mixed-phase processes in the computational domain. A constant and uniform updraft w is also assumed. Thus, no feedback mechanisms between dynamical and microphysical processes are simulated. Moreover, all the variables are considered uniform in the horizontal and the problem is unidimensional in z. The eqs. (23) are solved numerically by using the upstream scheme for the advective part and assuming zero vertical gradients at the lower boundary. The source-sink terms on the right hand side of the equations are treated with a simple explicit scheme.

Fig. 6 displays time-height cross-sections of temperature, condensate and fractional ice content for a 8-h integration with $w = 0.10\ m\ s^{-1}$. Fig. 6a shows that the air is constantly cooled by adiabatic ascent. This effect is partly balanced by the release of latent heat due to microphysical conversion processes, but a net cooling of the entire column is visible as time elapses. The development of an isothermal structure at the end of the simulation is an effect of the lower boundary condition. At the beginning of the integration, the temperature changes from 4°C at cloud base to $-5°C$ near the top. Thus, during the first 2 h of the integration both warm rain and cold cloud processes are active. Subsequently, the temperature of the entire layer becomes below freezing and only mixed or glaciated clouds can be simulated. Fig. 6b shows that M is generated early in the integration. As time elapses, M grows mostly from vapor deposition on ice crystals, and a quasi equilibrium is quickly established characterized by a vertically stratified structure.

Using the equilibrium version of (20), the fractional ice content was calculated and the result is presented in Fig. 6c. The solid phase is confined to regions with $T < 0°C$, an assumption built into the cloud scheme. However the liquid phase can exist as SLW below 0°C and mixed phase is apparent during most of the integration time. During the early part of the simulation the SLW constitutes more than half of the condensate ($f < 0.5$), and the solid phase gradually builds up as time elapses. The simulated SLW $[(1-f)M]$ generally remains below $0.1\ g\ m^{-3}$ and values between 0.02–$0.06\ g\ m^{-3}$ persist between 2 and 5 hours at cloud base. These roughly correspond to

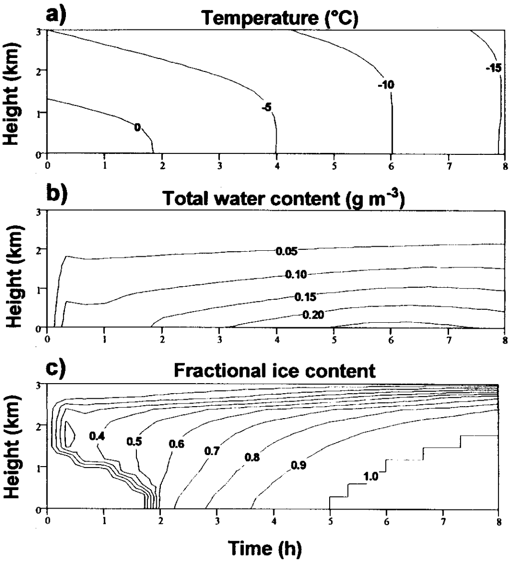

Fig. 6. Layer cloud integration of the cloud scheme with $w = 0.10\ m\ s^{-1}$, showing (a) temperature, (b) total water content, and (c) fractional ice content contoured versus time (h) (abscissa) and altitude (km) (ordinate).

a rain intensity of 0.2 to $0.8\ mm\ h^{-1}$ [using a M–R relationship given by Kessler(1969)] suggesting a significant freezing drizzle episode at cloud base. For temperature above freezing M is interpreted as liquid precipitation so rain falls out from the lower boundary. During the first 2 h of simulation (Fig. 6b) a rain episode is simulated at cloud base [$M \approx 0.15\ g\ m^{-3}$ ($2\ mm\ h^{-1}$)]. Subsequently, there is a transition from rain to snow (for example between $t = 2$ h and $t = 5$ h at the cloud base). During this time interval, the phase of condensate is significantly mixed especially during the early time of the transition where M mostly consists of SLW.

To illustrate the sensitivity of the scheme to the intensity of the vertical velocity, Fig. 7 depicts vertically integrated values of M, q_S, q_L, and SLW, for $w = 0.01$, 0.10 and $0.50\ m\ s^{-1}$. These diagrams indicate that SLW has a transient behavior, and is a significant contributor to the total mass of condensate. In general, strong updrafts (Fig. 7c) result in large values of SLW over short time intervals, and small w (Fig. 7a) support weaker SLW signals but over longer intervals of time. Note that for vertical velocities representative of large-scale ascents (Fig. 7a) SLW can last for relatively long periods of time (≈ 36 h).

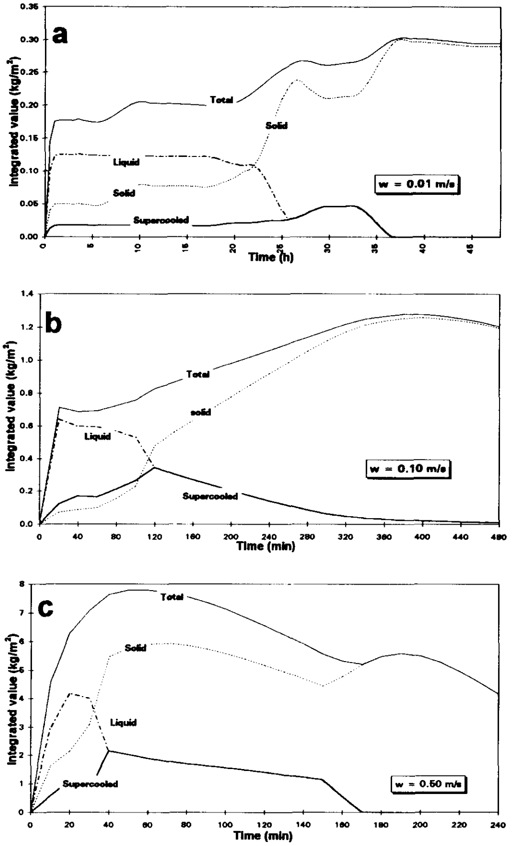

Fig. 7. Vertically integrated water substances as functions of time for layer clouds simulations with $w = 0.01$, 0.10 and 0.5 m s^{-1}. The "liquid" curve refers to the total amount of liquid phase and the "supercooled" curve indicates the amount of liquid at subfreezing temperature. Note the different time scale in each diagram.

5. Mesoscale MC2 integrations

To provide an example of the behavior of the present cloud scheme on the mesoscale, a more complete numerical experiment will be briefly discussed. The fully compressible, three-dimensional, non-hydrostatic, semi-implicit and semi-Lagrangian (SISL), MC2 (mesoscale compressible community) model was used as the basic framework for a first implementation of the mixed-phase cloud scheme. The MC2 model originated from a regional hydrostatic model (Robert et al. 1985). It was generalized to the Euler system by Tanguay et al. (1990), and successfully applied to synoptic storm simulations. Subsequently, the same model was used at fine-scale by Robert (1993) for bubble convection experiments and Tremblay (1994) for squall-line simulations, emphasizing the *universal* nature of this dynamical framework. Some characteristics of MC2 include: variable vertical resolution, modified Gal-Chen terrain-following scaled-height vertical coordinate, a limited-area one-way nesting strategy, and a complete physics package (Benoit et al., 1989). Its main asset among existing non-hydrostatic models is its novel SISL formulation (Laprise, 1995)

The winter storm chosen for simulation occurred on 14 of March 1992 over the north Atlantic, near the Canadian east coast. To simulate the development of this storm, a 24-h MC2 forecast at 50 km resolution initialized at 00 UTC 14 March 1992 was generated. These data were used to drive nested simulations (at 20 km and 10 km resolution). The domain was 2400×2600 km^2 for the 20 km simulation and 1400×2100 km^2 for the 10 km run. Only the results of the 20 km integration will be discussed below.

Several preliminary tests have been performed with the MC2 model including the mixed-phase cloud scheme. These have demonstrated the insensitivity of model results to timestep (halving the time step did not affect the results) and domain size and resolution (doubling the resolution and extending the domain neither produced additional features nor changed these already present).

Even if a formal validation of the present scheme is beyond the scope of this paper, it is nevertheless useful to have some indications of its general behavior. To address this issue, simple comparisons with observations at the validation time were made. It was found that the 24-h forecast captures fairly well the central value of the low pressure system (976 mb versus 975 mb observed) and that the 500 mb biases of temperature, geopotential and wind speed were 0.3°C, 6 dm and 6 m s^{-1}, which is roughly comparable with other mesoscale models (Gyakum et al., 1995). A more formal validation is a logical step to the present work, and should consider detailed surface analysis and extensive use of satellite information (Alliss et al., 1993; Raustein et al., 1991). Since the present scheme forecasts mixed-phase clouds an additional effort should be made toward a validation with respect to recent aircraft measurements of such clouds (Moss and Johnson, 1994; Cober et al., 1995a).

MC2 24-h forecasts of vertically integrated solid, warm liquid and supercooled liquid water content generated with the mixed-phase cloud scheme are depicted in Fig. 8. The strongest portion of the signal is located near the low center where both solid and warm liquid phases are in excess of 0.8 kg m^{-2}. Near this location the SLW integral exceeds 0.1 kg m^{-2} over a localized region of the domain. In this region, an occlusion process is almost completed and a narrow tongue of warm air with surface temperature above freezing is spiraling around the low center. This configuration and a strong updraft core are responsible for this important episode of warm, solid and freezing precipitation. At a larger scale, there is a wide elongated band associated with a cold front where both integrated solid and liquid phases are within a range of 0.2 to 0.8 kg m^{-2}. In the same region the SLW signal always remains below 0.2 kg m^{-2}. In general the SLW signal is weak and localized and represents only a small portion of the total mass of condensate.

Fig. 9 illustrates the relative contribution of the different phases by showing total integrated

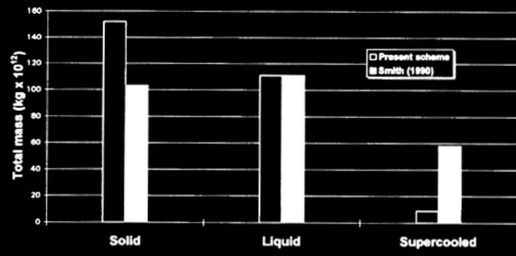

Fig. 9. Total mass for different phases of condensate calculated with the present scheme and with the fractional ice content given by Smith (1990).

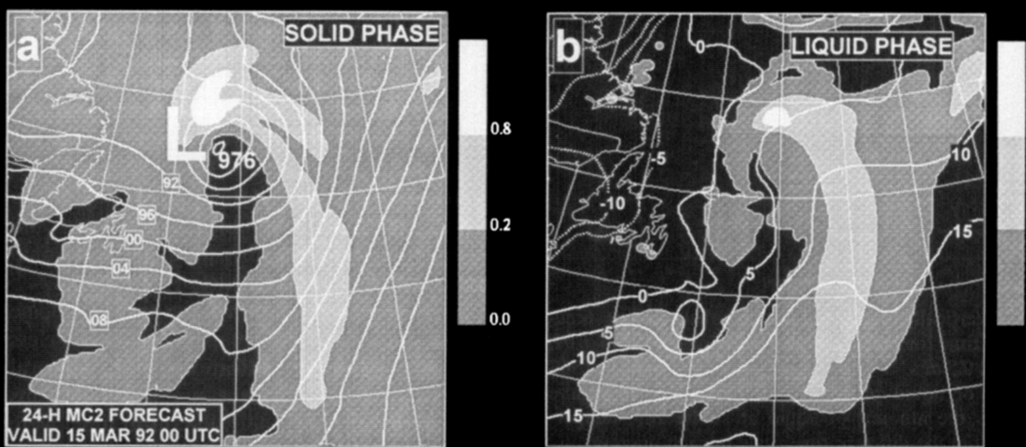

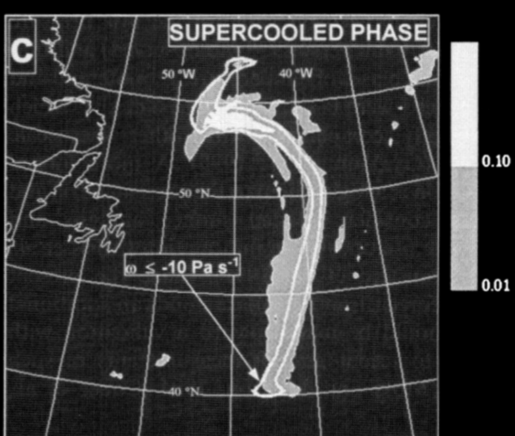

Fig. 8. Vertically integrated (a) solid water content superimposed with sea level pressure (contoured at each 4 mb); (b) liquid water content superimposed with surface temperature (contoured at each 5°C, dashed negative); (c) supercooled water content superimposed with the outline of isobaric vertical velocity at $z = 3$ km (the tick contour line delineates regions where $\omega \leqslant -10$ Pa s^{-1}). The unit of the integrated water content is kg m^{-2}.

masses in the three-dimensional domain. The figure shows that present scheme distributes M as 56% of solid, 41% of warm liquid and 3% of SLW. To provide a comparison with other schemes currently used in general circulation models, Fig. 9 also depicts the partition of M calculated with the scheme suggested by Smith (1990):

$$1-f \equiv f_L = \begin{cases} \frac{1}{6}\left[\frac{T+15}{5}\right]^2 & -15°C < T < -5°C, \\ 1 - \frac{1}{3}\left(\frac{T}{5}\right)^2 & -5°C \leqslant T < 0°C. \end{cases} \tag{28}$$

It is clear from Fig. 9 that (28) generates a SLW mass larger by a factor 6 with respect to the present scheme. Of course this translation of the SLW mass is at the expense of the solid phase mass. Thus, grouping warm liquid and supercooled phases together, the mixed-phase cloud scheme distributes the total mass of condensate into 56% for solid and 44% for liquid. On the other hand equation (28) gives 38% for solid and 62% for liquid. Such a difference is significant and may be important enough to affect the results of long term integrations, since there is a substantial contrast between the radiative properties of liquid and ice clouds.

The reader should note that these results are very preliminary, and as mentioned above, a formal validation must be considered in order to make this comparison reliable. However, it is felt that the mixed-phase scheme is in qualitative agreement with aircraft data presented by Tremblay et al. (1995) and Cober et al. (1995). It was shown in these studies that the SLW is a very localized and a small-scale phenomenon, suggesting that Fig. 8c may be representative of SLW distribution found in North Atlantic winter storms. More recently, Tremblay et al. (1996) have shown, based on SSM/I data, that forecast techniques for SLW using simpler indicators (such as w, RH and T) contradict these measurements and systematically include glaciated clouds in SLW forecasts.

Fig. 10 illustrates the distribution of the fractional ice content in the mesoscale integration. Fig. 10a shows that f is highly localized and associated with the smallest scales of the model. More specifically, the supercooled phase is mostly confined to a narrow band ($\cong$ 100 km) associated with a region of strong frontal lifting. Within this band, near the crest of the thermal wave $f<0.5$, so M is mostly constituted of SLW in this region. Fig. 10b indicates that this band persists to an altitude where $T \cong -20°C$.

6. Summary and conclusions

In this paper, a novel approach for modeling mixed-phase clouds in NWP models and GCMs has been suggested. Considering microphysical parameterization schemes currently used in many CRMs, two equations for the time evolution of liquid and solid water content were established. From these equations an expression was derived for the partition of the total condensate into liquid and solid part, expressed as a fractional ice content. The analysis of the transient solutions of this equation allowed considering the equilibrium solutions only, and a diagnostic relationship for the fractional ice content was derived. Thus the mixed-phase cloud scheme includes only one prognostic variable: the total condensate and one diagnostic variable: the fractional ice content. The fractional ice content is inferred on a physical basis taking into consideration the value of large-scale parameters of temperature, vertical velocity, pressure, condensate amount and precipitation flux. Although highly simplified, the present scheme nevertheless preserves the basic microphysical processes characterizing natural mixed-phase clouds and does not include any adjustable (nonphysical) parameter.

The proposed approach, with only one prognostic variable (the total condensate) partitioned diagnostically into solid and liquid part, has the advantage of being computationally fast and easy to implement in mesoscale or large-scale atmospheric models. This allows simulations that would have been otherwise impossible with more elaborate cloud microphysics schemes.

The mixed-phase cloud scheme was tested in a one-dimensional model, in which a steady and uniform updraft was assumed to exist within an atmospheric layer. The generation and temporal evolution of SLW were analyzed and the transient behavior of SLW was demonstrated. It was shown that for weak updrafts typical of large-scale ascent, a low amplitude SLW signal can last for relatively long periods of time (> 1 day). For intense meso-

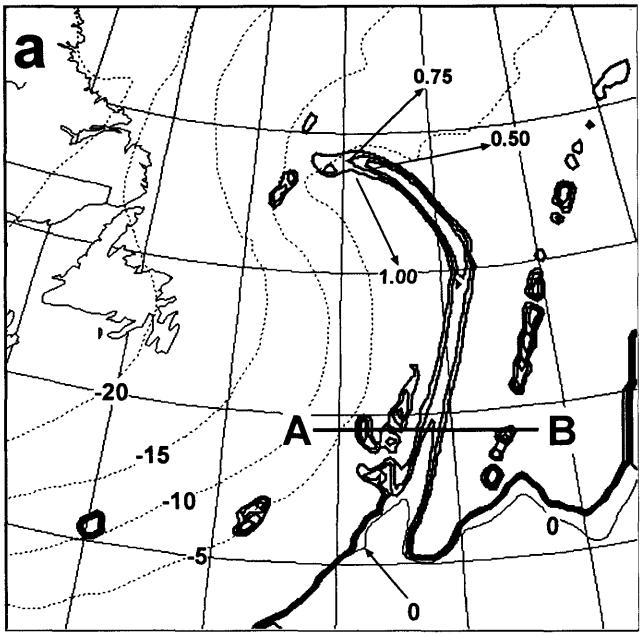

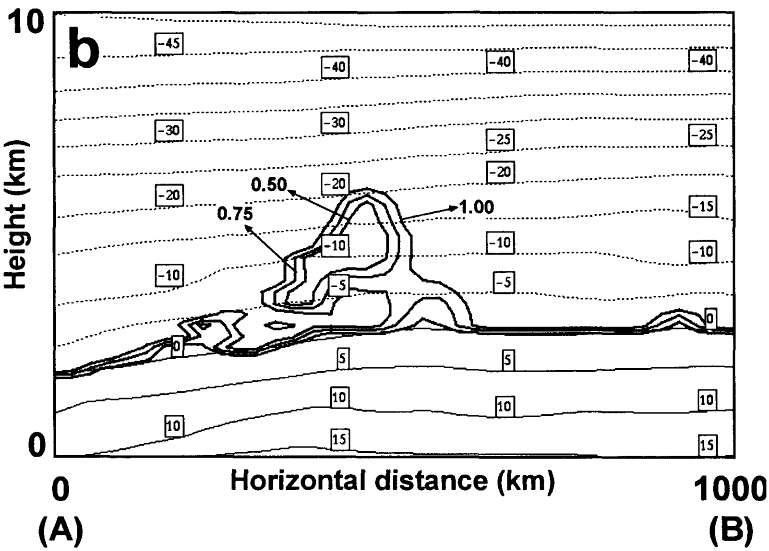

Fig. 10. A 24-h forecast of the fractional ice content superimposed with temperature: (a) at $z = 3$ km; (b) along the line segment AB. Only the first 10 km of the vertical domain are displayed.

scale updrafts, stronger SLW signals are generated but exist for short time intervals.

The cloud scheme was also implemented in the Canadian MC2 (Mesoscale Compressible Community) model and a numerical simulation of 14 of March 1992 winter storm over the north Atlantic, near the Canadian east coast, was discussed. As the scheme is not yet generalized for subgrid condensation, no fractional cloud cover is allowed and only high resolution ($\leqslant 20$ km) mesoscale simulations can be considered now, large-scale application being left for the future.

One of the results, obtained from the mesoscale simulations with the present scheme, is the temporal and spatial distribution of condensed water phases. The SLW occurs mainly as a localized phenomenon strongly correlated with the vertical lifting, and may be found even near the $-20°C$ isotherm. The SLW amount is substantially different from those obtained with other schemes using temperature as the only indicator for appearance of ice in supercooled water (Smith, 1990; Sundqvist, 1993). It was found that the formula of Smith (1990) tends to overestimate the SLW by a factor 6 with respect to our mixed-phase cloud scheme. It is felt that such a difference is large enough to affect the results of long term integrations.

The preliminary results obtained with the proposed scheme are encouraging. The results are reasonable and allow a consistent physical interpretation. However, a rigorous verification is essential to asses the validity of the proposed mixed-phase cloud scheme.

7. Acknowledgments

The authors are grateful to Professor Hilding Sundqvist, Dr. George Isaac, Professor Da-Lin Zhang and Dr. Stephane Laroche for commenting on this manuscript.

REFERENCES

Alliss, R. J., Sandlin, G. D., Chang, S. W. and Raman, S. 1993. Application of SSM/I data in the analysis of hurricane Florence (1988). *J. Appl. Met.* **32**, 1581–1591.

Asai, T. 1965. A numerical study of air-mass transformation over the Japan sea in winter. *J. Meteor. Soc. Japan* **43**, 1–15.

Benoit, R., Cote, J. and Mailhot, J. 1989. Inclusion of a TKE boundary layer parameterization in the Canadian Regional finite-element model. *Mon. Wea. Rev.* **117**, 1726–1750

Cober, S. G., Isaac, G. A. and Strapp, J. W. 1995. Aircraft icing measurements in east coast winter storms. *J. Appl. Met.* **34**, 88–100.

Cober, S., Isaac, G., Strapp, J. W. and Marcotte, D. 1995a. Icing environment associated with supercooled drizzle. *Proceedings, International Icing Symposium.* Montreal, Canada. Amer. Helicopter Soc.

Colton, D. E. 1976. Numerical simulations of the orographically induced precipitation distribution for use in hydrologic analysis. *J. Appl. Meteor.* **15**, 1241–1251.

Cotton, W. R. and Anthes, R. A. 1989. Storm and cloud dynamics. *International Geophysics Series* no. **44**. Academic Press. 883 pp.

Fletcher, N. H. 1962. *The physics of rainclouds.* Cambridge University Press, Cambridge. 386 pp.

Gyakum, J. R., Carrera, M., Zhang, D. L., Miller, S., Chouinard, C., Benoit, R., Buzzi, A., Krishnamurti, T. N., Kuo, Y. H., Lalaurette, F., Low-Nam, S., Mailhot, J., McGregor, J. M., Mesinger, F., Modica, G., Nakamura, M., Tripoli, G. and Wilson, C. 1995. First COMPARE Workshop, 3–5 October 1994, Montreal, Quebec, Canada. *Bull. Amer. Meteor. Soc.* **76**, 1209–1218.

Houze, R. A. 1992. Cloud dynamics. *International Geophysics Series*, no. **53**. Academic Press. 573 pp.

Kessler, E. 1969. On the distribution and continuity of water substance in atmospheric circulations. *Meteor. Monograph*, **10**. Amer. Meteor. Soc. 84 pp.

Koenig, L.R. and Murray, F. W. 1976. Ice-bearing cumulus cloud evolution: numerical simulation and general comparison against observations. *J. Appl. Met.* **15**, 747–762.

Laprise, R. 1995. The formulation of Andre Robert MC2 (Mesoscale Compressible Community) model. *Atmos. Ocean*, the A.J. Robert Symposium special issue, in press.

Lin, Y. L., Farley, R. D. and Orville, H. D. 1983. Bulk parameterization of the snow field in a cloud model. *J. Clim. Appl. Met.* **22**, 1065–1092.

Matveev, L.T. 1984. *Cloud dynamics.* D. Reidel Publishing Company. 340 pp.

Mellor, G.L. 1977. The Gaussian cloud model relations. *J. Atmos. Sci.* **34**, 356–358.

Moss, S. J. and Johnson, D. W. 1994. Aircraft measurements to validate and improve numerical model parameterisations of ice to water ratios in clouds. *Atmos. Res.* **34**, 1–25.

Ogura, Y. and Takahashi, T. 1971. Numerical simulation of the life-cycle of a thunderstorm cell. *Mon. Wea. Rev.* **99**, 895–911.

Orville, H. D. and Kopps, F. J. 1977. Numerical simulation of the life history of a hailstorm. *J. Atmos. Sci.* **34**, 1596–1618.

Pruppacher, H. R. and Klett, J. D. 1978. *Microphysics of clouds and precipitation.* D. Reidel Publishing Company, 714 pp.

Raustein, E., Sundqvist, H. and Katsaros, K. 1991. Quantitative comparison between simulated cloudiness and clouds objectively derived from satellite data. *Tellus* **43A**, 306–320.

Roads, J. O., Vallis, G.K. and Remer, L. 1984. Cloud/

climate sensitivity experiments. In *Climate processes and climate sensitivity.* Maurice Ewing Series, 5. J. E. Hansen and T. Takahashi (eds). Amer. Geophys. Union, Wash. D.C. 130–162.

Robert, A. 1993. Bubble convection experiments with a semi-implicit formulation of the Euler equations. *J. Atmos. Sci.* **50**, 1865–1873.

Robert, A., Yee, T. L. and Ritchie, H. 1985. A semi-Lagrangian and semi-implicit numerical integration scheme for multilevel atmospheric models. *Mon. Wea. Rev.* **113**, 388–394.

Rogers, R. R. 1979. *A short course in cloud physics.* International Series in Natural Philosophy. Pergamon Press. 235 pp.

Rutledge, S.A. and Hobbs, P. V. 1984. The mesoscale and microscale structure and organization of clouds and precipitation in midlatitude cyclones. XII: a diagnostic modeling study of precipitation development in narrow cold-frontal rainbands. *J. Atmos. Sci.* **41**, 2949–2972.

Smith, R. N. B. 1990. A scheme for predicting layer clouds and their water content in a general circulation model. *Quart. J. Roy. Met. Soc.* **116**, 435–460.

Sommeria, G. and Deardorff, J. W. 1977. Subgrid-scale condensation in models of non-precipitating clouds. *J. Atmos. Sci.* **34**, 344–355.

Stewart, R. E. and Crawford, R. W. 1995. Some characteristics of the precipitation formed within winter storms over eastern Newfoundland. *Atmos. Res.* **36**, 17–37.

Sundqvist, H. 1978. A parameterization scheme for non-convective condensation including prediction of cloud water content. *Q. J. R. Meteor. Soc.* **104**, 677–690.

Sundqvist, H. 1981. Prediction of stratiform clouds: Results from a 5-day forecast with a global model. *Tellus* **33**, 242–253.

Sundqvist, H. 1993. Inclusion of ice phase of hydrometeors in cloud parameterization for mesoscale and largescale models. *Beitr. Phys. Atmosph.* **66**, 137–147.

Sundqvist, H., Berge, E. and Kristjansson, J. E. 1989. Condensation and cloud parameterization studies with a mesoscale numerical weather prediction model. *Mon. Wea. Rev.* **117**, 1641–1657.

Tanguay, M., Robert, A. and Laprise, R. 1990. A semi-implicit semi-Lagrangian fully compressible regional forecast model. *Mon. Wea. Rev.* **118**, 1970–1980.

Tiedtke, M. 1993. Representation of clouds in large-scale models. *Mon. Wea. Rev.* **121**, 3040–3061.

Tremblay, A. 1994. Simulations of the 14 July 1987 squall line using a fully compressible model. *Atmos. Ocean* **32**, 567–603.

Tremblay, A., Glazer, A., Szyrmer, W. and Yu, W. 1994. Mesoscale simulations of cloud microphysics within a winter storm: some implications for large-scale ice phase schemes. Proceedings, *ECMWF/GCSS Workshop on modelling and assimilation of clouds.* 31 October–4 November, 1994. Reading UK, pp. 337–346.

Tremblay, A., Glazer, A., Szyrmer, W., Isaac, G. and Zawadzki, I. 1995. Forecasting of supercooled clouds. *Mon. Wea. Rev.* **123**, 2098–2113.

Tremblay, A., Cober, S., Glazer, A. and Isaac, G. 1996. An intercomparison of mesoscale forecasts of aircraft icing using SSM/I retrievals. *Weather and Forecasting* **11**, 66–77.

Zawadzki, I., Ostiguy, L. and Laprise, R. 1993. Retrieval of the microphysical properties in a CASP storm by numerical integration of a kinematic model. *Atmos. Ocean* **31**, 201–233.